Article

Various Grids in Moiré Measurements

Vladimir Saveljev *

Posted Date: 12 September 2024

doi: 10.20944/preprints202409.0979.v1

Keywords: moiré effect; moiré measurements; moiré magnifier; public safety

 doi:10.20944/preprints202409.0979.v1

Article

Various Grids in Moiré Measurements

Vladimir Saveljev

Public Safety Research Center, Konyang University, Nonsan, Republic of Korea; saveljev.vv@gmail.com

Abstract: The moiré effect is typically observed in regular periodic structures and sometimes in random (aperiodic) structures. However, only regular structures were used in measurements. In this study, we propose structures whose images are not regular but not completely random, and resemble a series of lines, such as a grid of dotted lines or a matrix of dots. A relatively simple image processing technique can make the moiré effect in such structures very similar to regular structures. We demonstrated using five different structures (including text) in measurements, with similar results.

Keywords: moiré effect; moiré measurements; moiré magnifier; public safety

1. Introduction

Moiré is an effect that forms patterns with a longer spatial period as a result of interference of projections of similar periodic structures with shorter periods [1–5]. The effect is usually considered in coplanar layers [1,2,6–8], i.e., in two dimensions; sometimes, the moiré effect is studied in 3D [9–12].

The moiré effect is mainly studied in regular structures but sometimes in approximate [13] or random [14,15] structures.

A useful particular application of the moiré effect is the measurement of displacement of distant objects by optical methods [16–20] using, for example, a digital camera. Moiré measurements are usually relative, i.e., the object's position is measured relative to a specific reference point. Measuring displacement with a digital camera using the moiré effect has advantages over direct linear measurements because of the moiré magnification [21,22].

Previously, we proposed a deferred moiré method for measuring displacements using a digital camera [23]. This method is based on moiré magnification [21] and phase proportionality [1]. The magnification means improved sensitivity, and the phase of the patterns means displacement. For moiré measurements, there must be two grids: a grid on the measured object and a static reference grid. In our method, the computer generates the second grid. Calibration is not needed because the size of the grid attached to the object is known.

The physically measured phase is always within the interval $[-\pi, \pi]$, similar to the principal value of multi-valued trigonometric functions (arcsine and arctangent). This effect is called folding or wrapping, and looks graphically like a folded paper fan or an accordion's expanding/contracting bellows. Wrapping is a form of ambiguity. However, the resulting measured phase should be definite and unambiguous. Therefore, unwrapping (unfolding) is necessary for practical measurements. This can be achieved by tracking peaks, phase unwrapping [24,25] or other methods.

Given that the moiré effect is an integral effect (it can be expressed as a convolution integral) [1], the grids do not necessarily consist of only solid straight lines. They just need to maintain some periodicity "on average". Thus, similar to approximate gratings [13], the lines of graphic objects can be dotted, zigzagged, etc., as long as the "traces" of the lines are preserved; that is, such objects should be "arranged in parallel rows". We avoided the influence of a particular structure by using a profile averaged over one dimension. Therefore, we are actually considered some kind of one-dimensional moiré effect.

 doi:10.20944/preprints202409.0979.v1

The paper is arranged as follows: Section 2 briefly describes the measurement method. Section 3 introduces approximate grids and similar objects, and demonstrates measurements using these objects. Sections 4 and 5 contain the discussion and conclusion.

2. Materials and Methods

The moiré patterns arise in the region where two transparent grids overlap (superimpose) with each other; in this region, a low-pass filter (in the simplest case, averaging) is also applied. The dotted line at the center of Figure 1a shows the result. The moiré patterns in the grids with parallel lines are parallel to the grid lines. Therefore, to estimate the moiré patterns in such grids, it is sufficient to consider the vertical cross-section of the grids. The cross-section (profile) along the vertical line l is shown in Figure 1b. Such a one-dimensional profile completely describes the moiré effect in grids with parallel lines.

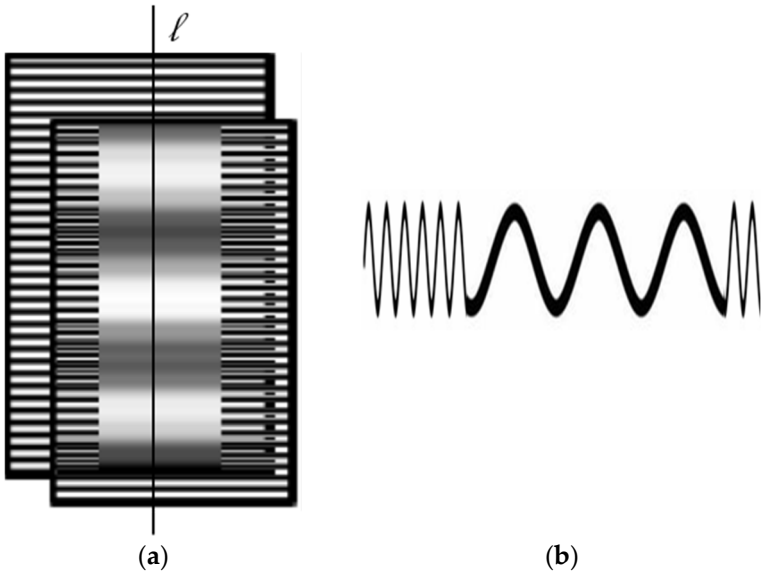

Figure 1. (a) Moiré patterns in grids with parallel lines. (b) Cross-section (profile) along line *l*.

In the moiré measurement system, a grid is attached to an object whose displacement (vibration) is measured. The camera is installed separately (with vibration insulation from the object), as shown in Figure 2. The phase of the moiré patterns is linearly proportional to the grid displacement. The physically measured value is the difference between the heights of the camera and the grid (effectively, the vibration averaged over the grid area). In the system [23], a static computer-generated grid provides a common reference for the measurement throughout the video.

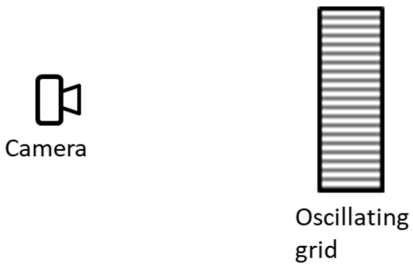

Figure 2. Scheme of measurement.

The flow charts of the processing algorithms are shown in Figure 3.

Preprints.org (www.preprints.org) | NOT PEER-REVIEWED | Posted: 12 September 2024 doi:10.20944/preprints202409.0979.v1

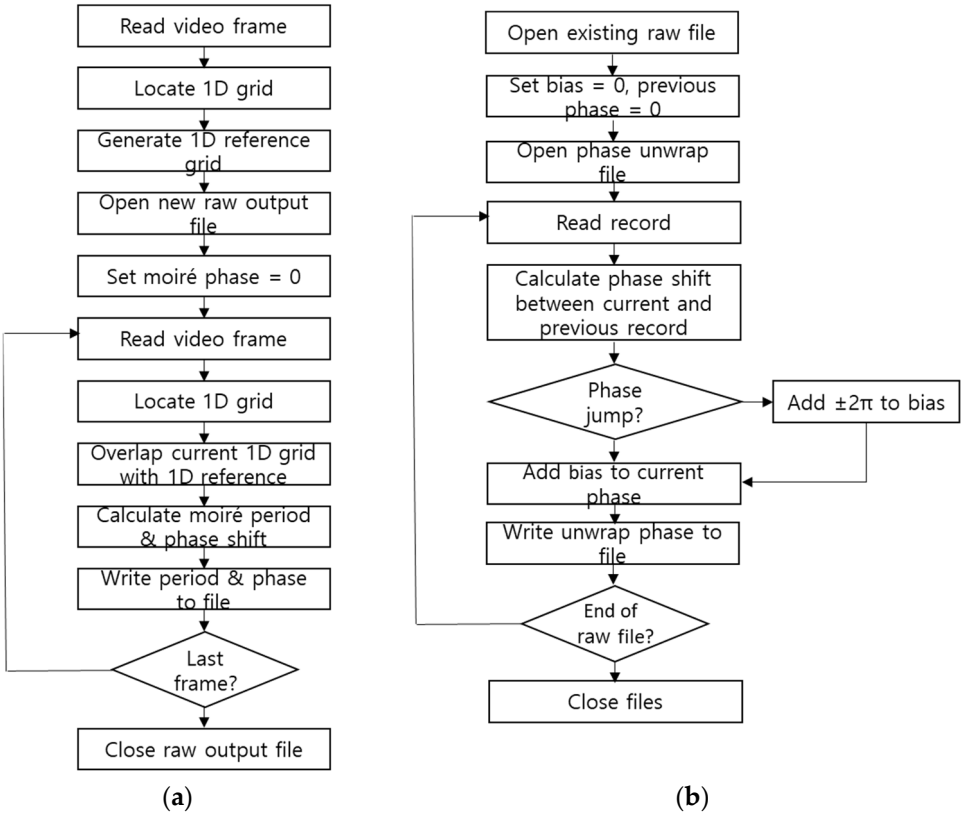

Figure 3. Flow charts of algorithms. (a) Image processing. (b) Phase unwrapping.

In the start-up process, the first video frame is displayed in a pop-up window, and the start and end points of the initial cross-section can be located interactively. Accordingly, we generate a common 1D reference grid (array) for the entire video sequence. Then, we read all video frames and superimpose the current grid (using the points captured in the start-up) on the reference grid. The overlapped area is then filtered using a Gaussian filter, and moiré patterns are obtained. Their period and phase of each video frame are written to the raw file. In the second stage, the raw phase is unwrapped by adding/subtracting the period corresponding to the sign of the phase jump between the current and previous frames, as in [26].

3. Results

Previously, we considered grids with a rectangular profile consisting of solid straight lines, as shown in Figure 4a. The grid's profile, i.e., its cross-section along a line l perpendicular to the grid lines (in this example, vertical), is shown in Figure 4b (the intensity is measured in 8-bit arbitrary units from 0 to 255). The profile is the same for all parallel vertical lines within the grid region.

Preprints.org (www.preprints.org) | NOT PEER-REVIEWED | Posted: 12 September 2024 doi:10.20944/preprints202409.0979.v1

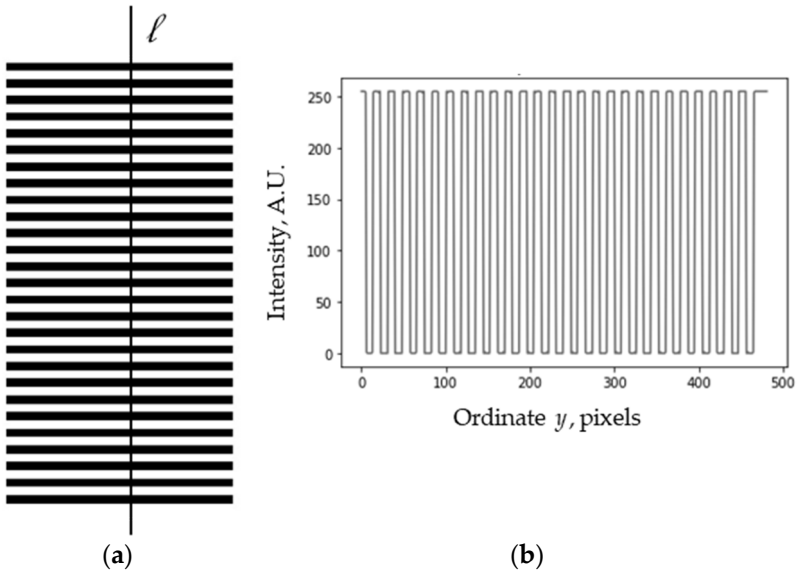

Figure 4. (a) Line grid consisting of solid lines. (b) Profile along line *l*.

3.1. Approximate Grids

Other regular structures, such as a dot matrix shown in Figure 5a, can also be used to observe the moiré effect. In this case, the profiles along different lines are different; see Figures 5b,c.

To eliminate the influence of such irregularity, we can, for example, consider the values obtained by summation along horizontal lines, as shown in Figure 5d. Such an averaged profile does not depend on the horizontal coordinate.

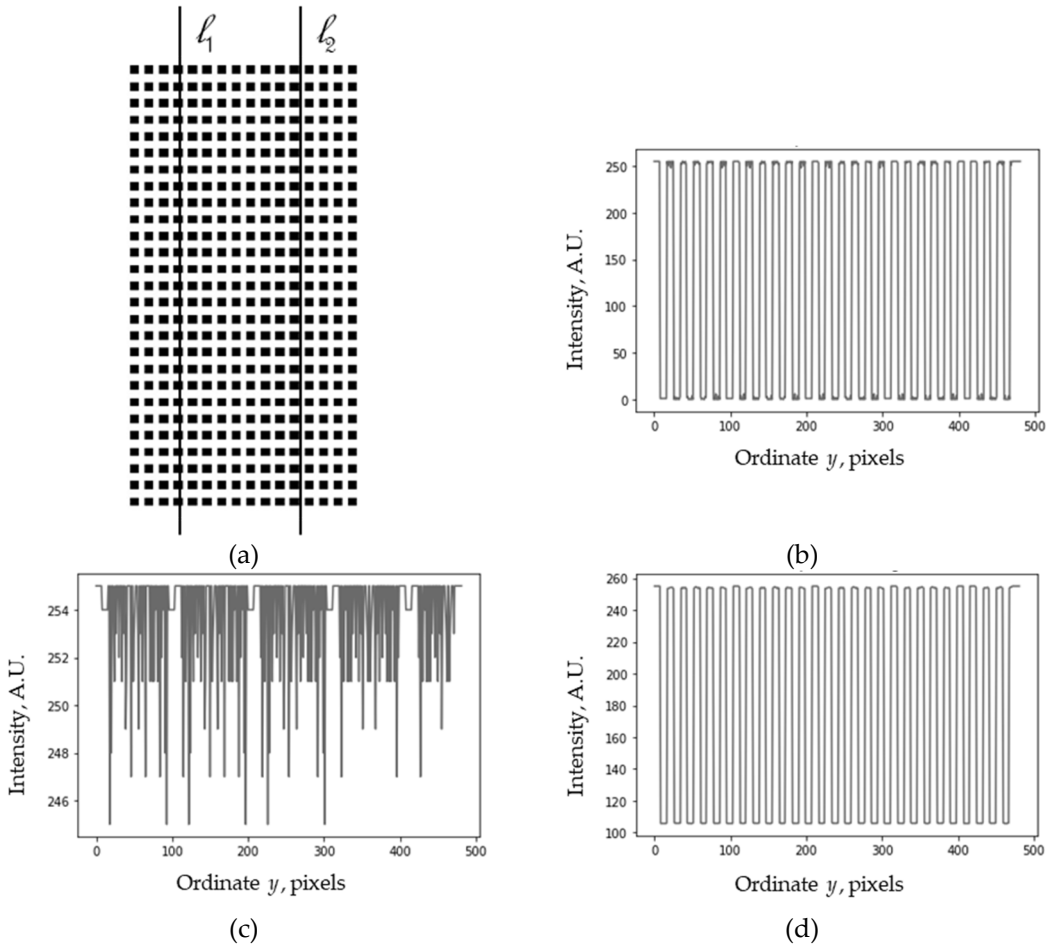

Preprints.org (www.preprints.org) | NOT PEER-REVIEWED | Posted: 12 September 2024 doi:10.20944/preprints202409.0979.v1

Figure 5. (a) Matrix of square dots. (b), (c) Its profiles along lines l_1 *and* l_2 ($x_1 = 48$, $x_2 = 120$). (d) Averaged profile.

Besides regular grids, we can also consider "distorted" nearly regular structures arranged in rows. For example, the pattern in Figure 6a consists of short segments of straight lines lying at the same height in each row. Also, some of the black squares of the square grid can be recolored or even removed, as in Figure 7a. In these cases, the profiles along different lines are different, see Figures 6b,c and 7b,c, but the periodic structure can be recognized in the averaged vertical profiles (obtained by summation along the rows), shown in Figures 6d and 7d.

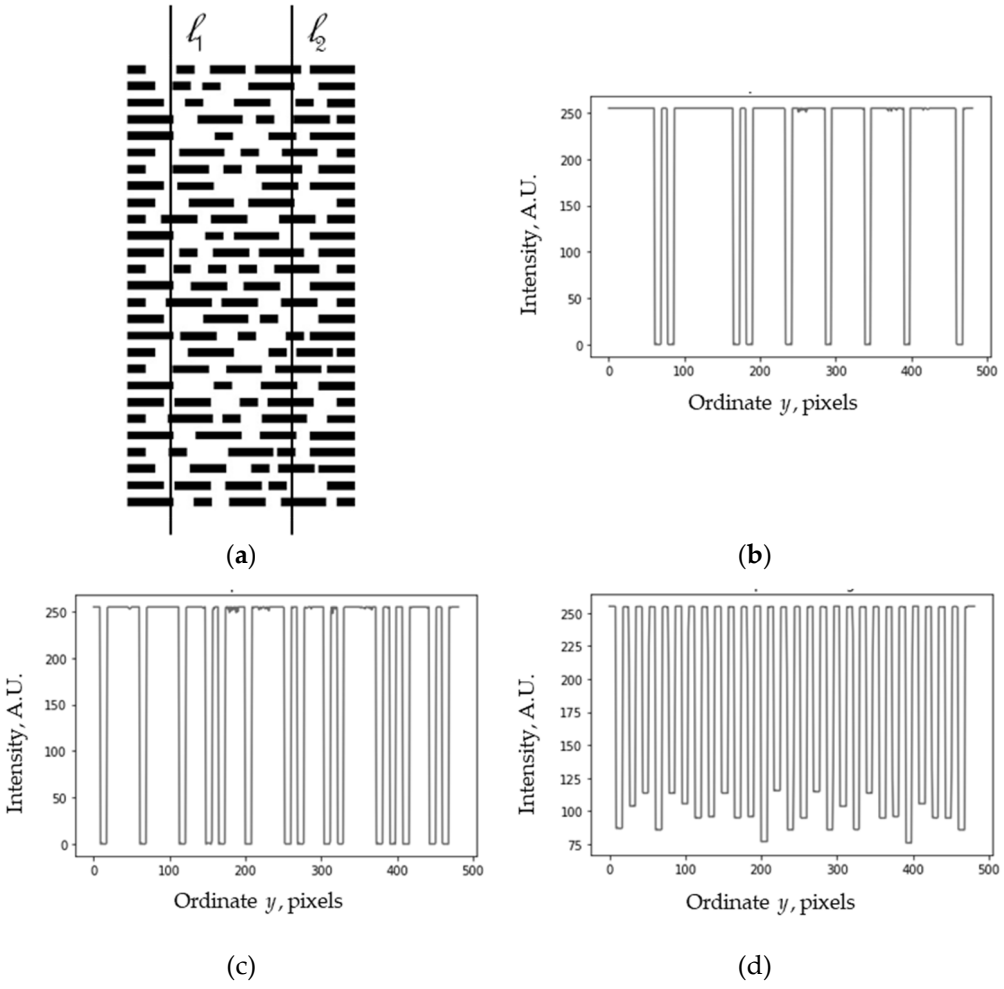

Figure 6. (a) Approximate dash grid. (b), (c) Its profiles along lines l_1 *and* l_2. (d) Averaged profile.

 doi:10.20944/preprints202409.0979.v1

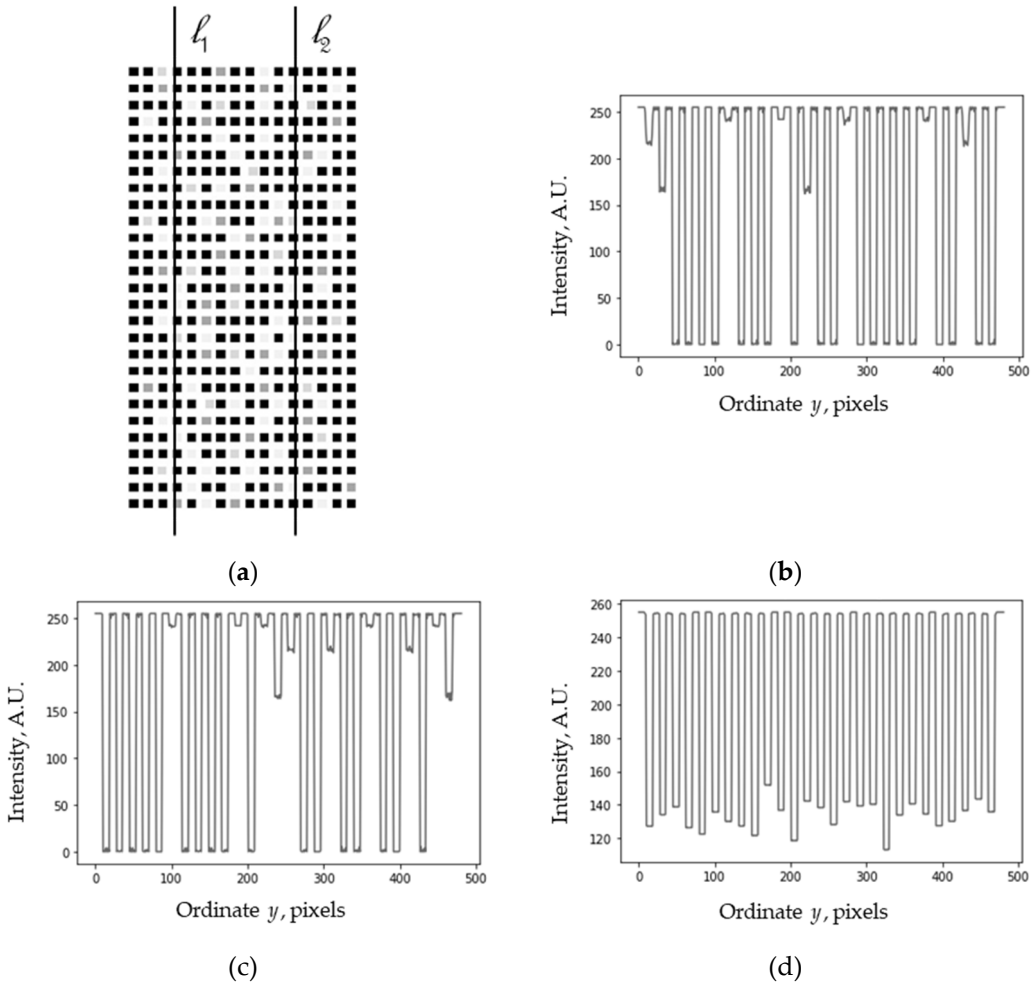

Figure 7. (a) Grayed square matrix. (b), (c) Its profiles along lines l_1 *and* l_2. (d) Averaged profile.

The averaged profiles are not strictly periodic but are nevertheless close to it. Later, we will see that this has almost no effect on the moiré measurements.

3.2. Other Objects as Grids

Some other structures organized into "lines," such as text, can also be used; see Figure 8a. This is an excerpt from a dummy placeholder text "lorem ipsum" in Latin [27]. Again, although the cross-sections are different (Figures 8b,c), the averaged profile in Figure 8d is close to periodic, except for some narrow peaks. This is similar to the dashed lines or the gray dot matrix, although the averaged profile of the text is less regular.

Preprints.org (www.preprints.org) | NOT PEER-REVIEWED | Posted: 12 September 2024 doi:10.20944/preprints202409.0979.v1

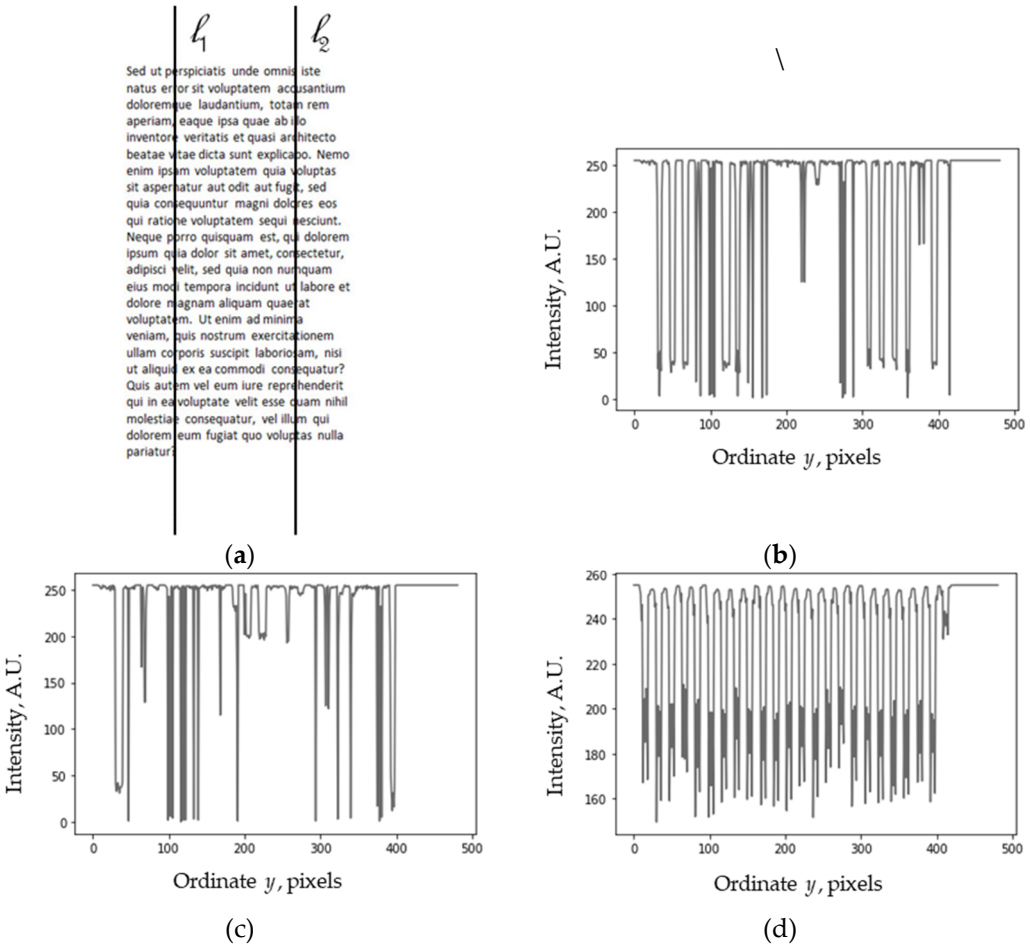

Figure 8. (a) Latin text lorem ipsum. (b), (c) Its profiles along lines l_1 *and* l_2. (d) Average by rows.

Text in other languages is also usually arranged in parallel rows (see the example of lorem ipsum in Korean [28] in Figure 9), and thus can also be used for moiré. As before, while the individual profiles (cross-sections) shown in Figures 9b,c are almost random, the averaged profile, especially its 'upper' part, appears close to regular, and the periodic structure is also recognizable.

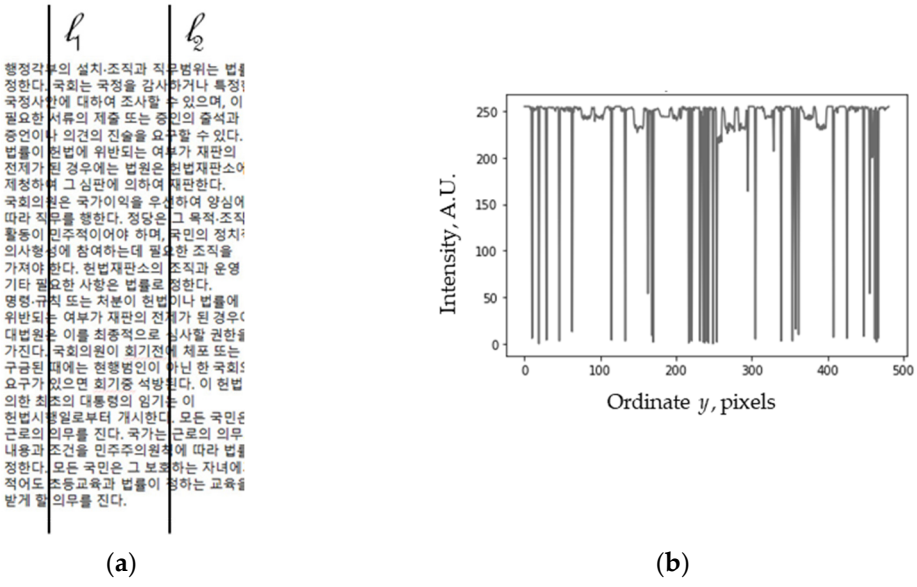

 doi:10.20944/preprints202409.0979.v1

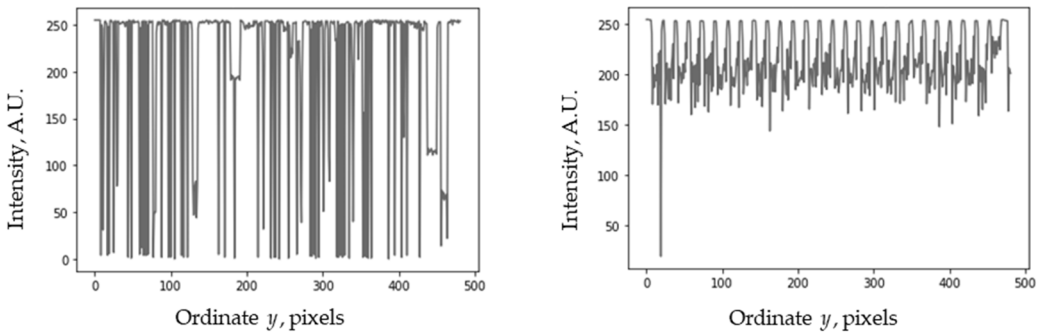

(c) (d)

Figure 9. (a) Korean text lorem ipsum. (b), (c) Its profiles along lines l_1 *and* l_2. (d) Averaged profile.

All samples in Figures 5–9 are arranged in rows, i.e., they consist of horizontal "rows", although they may be almost random within the rows. The vertical sections of the grids are almost random functions, and the moiré patterns obtained from these profiles will also be random. However, in the averaged vertical profile (summation along the image lines), the periodic structure is clearly recognizable. Therefore, their averaged profiles help to obtain a uniform moiré effect independently of the internal structure of the "rows" and, therefore, can be used for moiré measurements as a one-dimensional grid in the same way as in Section 2.

3.3. Measurements Using Various Grids

The measurement scheme is essentially the same as in Figure 2; the general view (photographs) is shown in Figure 10. The image of the grid can be seen on the computer screen in Figure 10b.

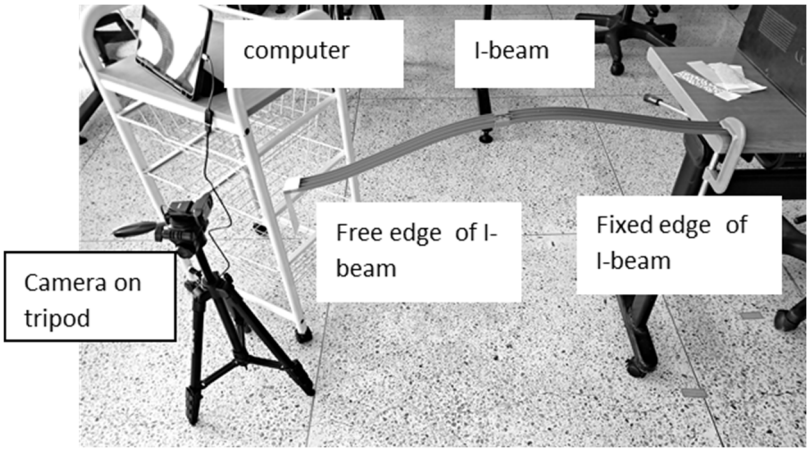

(**a**)

 doi:10.20944/preprints202409.0979.v1

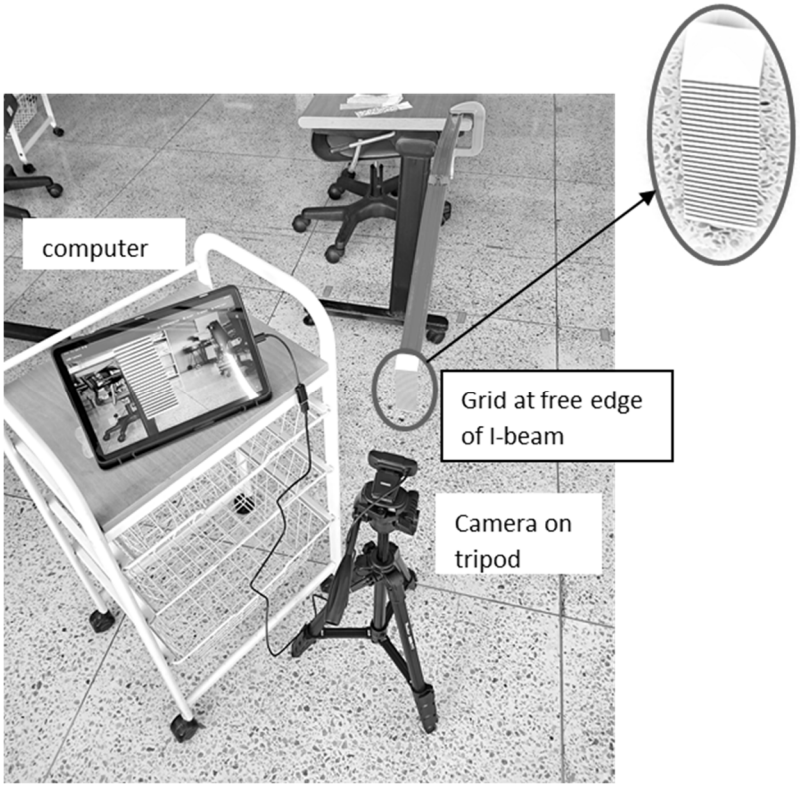

(**b**)

Figure 10. The layout of the measurement system (photographs from different directions).

In experiments, we used a Samsung Galaxy Tab S9 FE (10.9″) tablet computer and an external webcam. The plastic rod (I-beam) length with one fixed edge was 88 cm, and its cross-section was 37x8 mm. A C-clamp fixed one edge of the rod on the table; the grid was attached at the free edge. The distance from the camera to the free edge of the rod was 25 cm. The size of the printed grid was 4x10 cm, and its period was 4.038 cm.

The vibration was excited by pushing the I-beam manually (using a similar plastic rod) approximately in the middle. The FHD video 1920x1080 (30 FPS) was recorded for about 1 min and with the regular line grid processed according to the algorithm described in Section 2. The typical size of the grid image was 480x260 pixels.

The averaged profile was used for the measurements in grids other than the line grid. Figure 11 shows the image processing algorithm modified for the averaged profile. Almost all the algorithm steps (the superimposition with the computer-generated grid, the measurement of the phase of the moiré patterns) remain exactly the same as for the line grid described in Section 2. The modified sections are outlined in bold.

 doi:10.20944/preprints202409.0979.v1

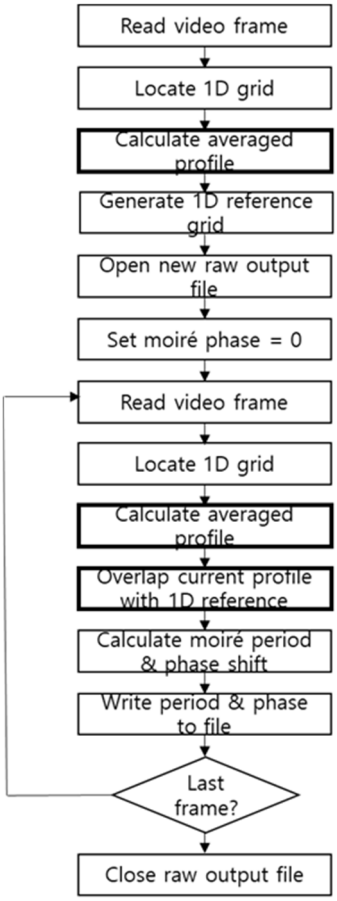

Figure 11. Flow chart of modified image processing algorithm for objects arranged in rows, such as approximate grids and text (compare to Figure 3b).

Photographed grids are shown in Figure 12. Illustrations of stages of processing are shown in Figure 13.

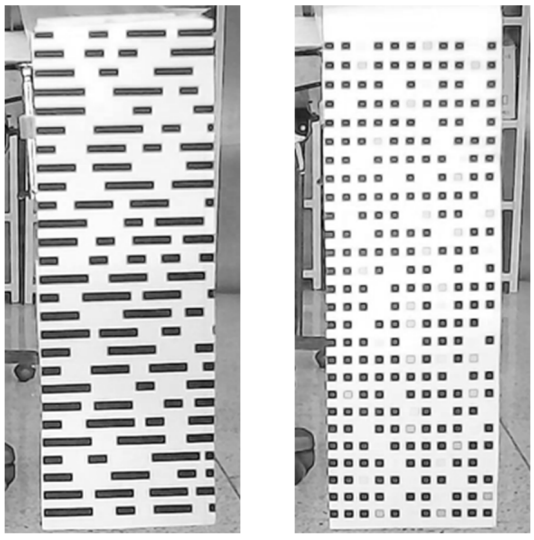

(**a**) (**b**)

Preprints.org (www.preprints.org) | NOT PEER-REVIEWED | Posted: 12 September 2024 doi:10.20944/preprints202409.0979.v1

(c) (d)

Figure 12. Photographed grids. (a) Dashed line, (b) Grayed square matrix, (c) Latin text, (d) Korean text.

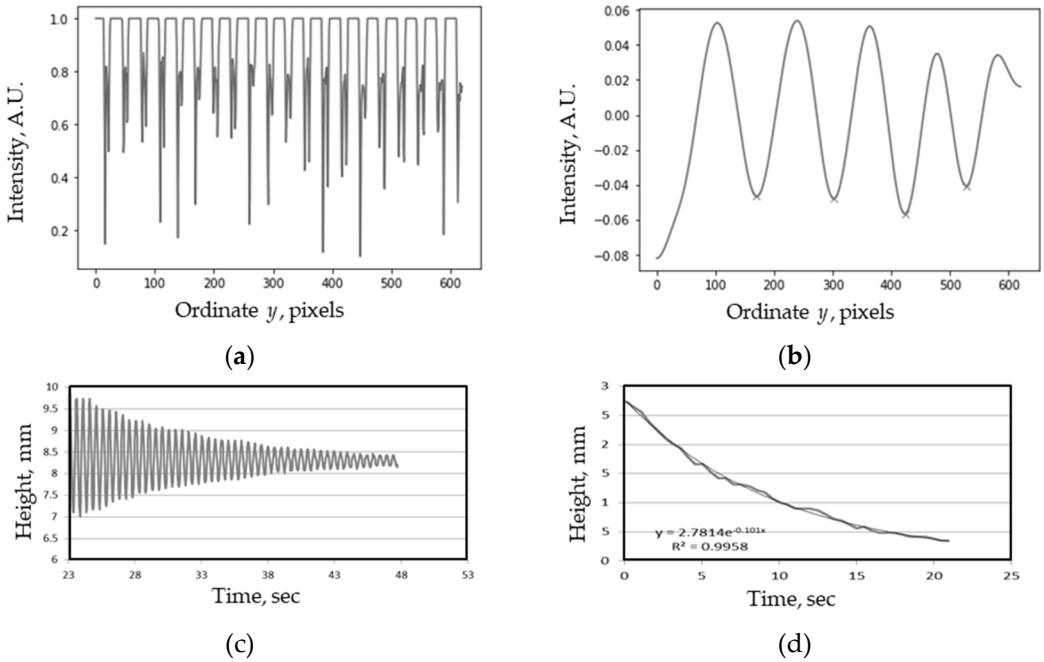

Figure 13. Stages of processing using an averaged profile. (a) Averaged profile. (b) Moiré patterns in averaged profile superimposed with a reference grid. (c) Measured oscillations. (d) Amplitude of oscillations.

In Figure 13c, the period was measured as the "horizontal" distance between successive maxima or minima, and the amplitude as the "vertical" distance between a maximum and the following minimum. The decrement was obtained from the amplitude plot by exponential regression.

The results of measurements using a regular grid and other objects arranged in parallel rows are given in Table 1.

Table 1. Results of measurements of the decaying oscillations in I-beam.

Grid	Period, sec	Standard deviation	Decrement, sec^{-1}	R^2 (coefficient of determination)
Line	0.495	3.4%	-0.094	0.993

 doi:10.20944/preprints202409.0979.v1

Dash	0.494	3.5%	-0.100	0.998
Square	0.493	4.0%	-0.104	0.987
Square gray	0.492	4.9%	-0.107	0.989
Latin text	0.495	5.6%	-0.111	0.986
Korean text	0.492	3.7%	-0.107	0.995
Mean	0.494	4.2%	-0.104	0.991
NRMSE	0.29%		5.87%	

The experiments show the following. The average measured period was 0.494 sec, and the average decrement was -0.104 sec^{-1}. (The oscillation frequency was 2.024 Hz with an average lifetime of 9.615 sec.) The normalized root-mean-square error (NRMSE) of the period was less than 0.3%, the NRMSE of the decrement was less than 6%, and the coefficient of regression R^2 was over 0.986, i.e., 98.6%. This means that the measurement results using all grids are pretty similar. Thus, the experiments demonstrate the reliability of moiré measurements of various objects arranged in rows using the averaged profile.

4. Discussion

Similar results for different objects arranged in rows were obtained, mostly because of the moiré effect's integral nature. Thus, the influence of narrow peaks mentioned in Section 3.2 was effectively eliminated.

However, more precise angular alignment was required in the approximate grids and text compared to the regular linear grid.

We have considered only five examples of objects arranged in rows. However, many more similar examples can easily be found, for example, in a slogan, a label, an advertisement, etc., on a bridge, a building, some equipment, and the like, and successfully used in practice.

The algorithm in Figure 3 has been implemented in real time [29]. Here, both stages (measuring the moiré phase and unwrapping it) were implemented in one pass. Therefore, the modified algorithm in Figure 11 for the objects arranged in rows can also be implemented in real-time.

5. Conclusions

We investigated the moiré effect in structures arranged in parallel rows. Despite the virtually random and completely different results obtained with conventional image processing, very similar results were obtained in various grids with a slight change in the processing method. This was demonstrated for five structures, including approximate grids and text in different languages. The results can potentially be applied to practical vibration measurements, where some structures arranged in parallel rows already exist on the object.

Funding: This research was funded by the National Research Foundation of Korea, grant number NRF2018R1A6A1A03025542.

Data Availability Statement: The original contributions presented in the study are included in the article, further inquiries can be directed to the corresponding author.

Acknowledgments: The author thanks the Priority Research Center Program for supporting this work through the National Research Foundation of Korea (NRF) funded by the Ministry of Education.

Conflicts of Interest: The author declares no conflicts of interest.

References

1. Amidror, I. The Theory of the Moiré Phenomenon, Vol. I, Periodic Layers, 2nd ed., Springer, 2009.
2. Bryngdahl, O. Moiré: Formation and interpretation. *J. Opt. Soc. Am.* **1974**, Vol. 64, No. 10, pp. 1287-1294.
3. Sciammarella, C.A. The moiré method - a review. *Exp. Mech.* **1982**, Vol. 22, No. 11, pp. 418-433.
4. Oster, G. *The science of moiré patterns*. Edmund Scientific, 1966.

5. Wu, Y.; Sun, M. 2D Moiré superlattice materials: Synthesis, properties and applications. *Appl. Mat. Today* **2024**, Vol. 37, p. 102101.
6. Hermann, K. Periodic overlayers and moiré patterns: theoretical studies of geometric properties. *J. Phys.: Condens. Matter* **2012**, Vol. 24, p. 314210.
7. de Jong, T.A..; Benschop, T.; Chen, X.; Krasovskii, E.E.; de Dood, M.J.A.; Tromp, R. M.; Allan, M.P.; van der Molen, S.J. Imaging moiré deformation and dynamics in twisted bilayer graphene. *Nat. Commun.* **2022**, Vol. 13, p. 70.
8. Dindorkar S.S.; Kurade, A.S.; Shaikh, A.H. Magical moiré patterns in twisted bilayer graphene: A review on recent advances in graphene twistronics. *Chem. Phys. Impact* **2023**, Vol. 7, p. 100325.
9. Saveljev, V. Moiré effect in 3D structures. In *Advances in Optics: Reviews*, Vol. 1, International Frequency Sensor Association (2018).
10. Kafri, O.; Glatt, I. *The Physics of Moiré Metrology*. Wiley-Interscience, 1990.
11. Weissman, Y. The 3D Moiré Effect for Fly-Eye, Lenticular, and Parallax-Barrier Setups. Pop3DArt, Israel, 2023.
12. Saveljev, V.; Kim, S.-K. Controlled moiré effect in multiview three-dimensional displays: image quality and image generation. *Opt. Eng.* **2018**, Vol. 57, No 6, p. 061623.
13. Saveljev, V.; Kim, J.; Son, J.-Y.; Kim, Y.; Heo, G. Static moiré patterns in moving grids. *Sci. Rep.* **2020**, Vol. 10, p. 14414.
14. Amidror, I. The Theory of the Moiré Phenomenon, Vol.II, Aperiodic Layers, 2nd ed., Springer, 2007.
15. Glass, L. Moiré effect from random dots. *Nature* **1969**, Vol. 223, pp. 578–580.
16. Patorski, K.; Kujawinska, M. *Handbook of the Moiré Fringe Technique.* Elsevier, Amsterdam, 1993.
17. Post, D.; Han, B.; Ifju, P. High Sensitivity Moiré: Experimental Analysis for Mechanics and Materials, Springer, New York, 1994.
18. Creath, K.; Wyant, J.C. Moiré and fringe projection techniques. In *Optical Shop Testing*, Malacara D. (Ed.), Second Edition, John Wiley & Sons, New York, 1992, pp. 653-685.
19. Khan, A.S.; Wang, X. Strain Measurements and Stress Analysis, Pearson, 2000.
20. Walker, C.A. (ed.). *Handbook of Moiré Measurement*, IOP Publishing, 2004.
21. Hutley, M.C.; Hunt, R.; Stevens, R.F.; Savander, P. Moiré magnifier. *Pure Appl. Opt. Part A* **1994**, Vol. 3, pp. 133–142.
22. Kamal, H;, Volkel, H..; Alda, J. Properties of moiré magnifiers, *Opt. Eng.* **1998**, Vol. 37, No. 11, pp. 3007-3014.
23. Saveljev, V.; Son, J.-Y.; Lee, H.; Heo, G. Non-contact measurement of vibrations using deferred moiré patterns. *Adv. Mech.Eng.* **2023**, Vol. 15, No. 4, pp. 1-11.
24. Qudeisat, M.; Gdeisat, M.; Burton, D.; Lilley, F. A simple method for phase wraps elimination or reduction in spatial fringe patterns. *Opt. Commun.* **2011**, Vol. 284, No 21, pp. 5105-5109.
25. Zuo, C.; Huang, L.; Zhang, M.; Chen, Q.; Asundi, A. Temporal phase unwrapping algorithms for fringe projection profilomery: a comparative review. *Opt. Lasers Eng.* **2016**, Vol. 85, pp. 84–103.
26. Gdeisat M.; Lilley, F. One-Dimensional Phase Unwrapping Problem. December **2010**. Available online: https://www.ljmu.ac.uk/-/media/files/ljmu/about-us/faculties-and-schools/fet/geri/onedimensionalphaseunwrapping_finalpdf.pdf (accessed on 23 June 2021).
27. Ostberg, R, Lorem ipsum. *Encyclopedia Britannica,* 10 Oct. **2023**. Available online: https://www.britannica.com/topic/Lorem-ipsum (accessed on 09 September 2024).
28. Hangeul Lorem Ipsum. Available online: http://guny.kr/stuff/klorem/ (accessed on 20 August 2024).
29. Saveljev, V.; Son, J.-Y.; Heo G. Using deferred moiré method for real-time measurements. In Proceedings of Korean Society of Civil Engineers, Convention, Conference & Civil Expo. Busan, Korea, 2022; pp. 7-8.